Journal of the Brazilian Society of Mechanical Sciences and Engineering (2025) 47:137
https://doi.org/10.1007/s40430-025-05433-z

TECHNICAL PAPER

Design and characterization of a magnetorheological elastomer linear actuator for low-frequency applications

Alberto Bellelli[1] · **Antonio Vairo**[1] · **Andrea Spaggiari**[1]

Received: 22 August 2024 / Accepted: 28 January 2025 / Published online: 21 February 2025

Abstract
This work presents the design and characterization of an innovative linear actuator for low-frequency applications based on a magnetorheological elastomer (MRE) disc coupled to an electromagnet. MREs are a class of smart materials in which micrometre-sized magnetic particles are suspended in an elastomeric matrix. Most research works study their applicability as semi-active systems, but less effort is devoted to their applicability in actuators, but their applicability in the field is possible and could lead to potential advantages in terms of integration of the system especially for microactuation. The proposed MRE device relies on a commercial electromagnet which provides linear motion of the MRE element. The stiffness of the elastomeric matrix is exploited to bring the system back to its initial position, so that the system is monostable. The magneto-mechanical behaviour is modelled both analytically and by means of finite element magneto-mechanical simulations, and the models are compared with the experimental tests. Two membrane thicknesses and two different gaps between the membrane and the electromagnetic actuator were manufactured and characterized. The results show the effect of the design variable on the actuator behaviour and confirm that the analytical model provided can predict the actuator's behaviour with a good approximation in all the configuration analysed. The dynamic range of the proposed system, regardless of the configuration selected, demonstrates that the magnetic contribution is always able to increase the actuator force by 50% and that the provided model can easily be used as a reliable design tool for this kind of smart system.

Keywords Magnetorheological elastomer · Design · Actuator · Finite element simulation

1 Introduction

Smart materials known as magnetorheological elastomers (MREs) have gained significant attention in recent years due to their unique ability to change their mechanical and rheological properties in response to magnetic fields. MREs are a semi-active material that combines elastomer properties and magnetorheological (MR) fluids, making them suitable for various applications, including dampers, sensors, and actuators. This article focuses on using MREs as an alternative to conventional actuators and explores their potential, combined with the commercial magnetic system, since the MRE itself is not able to produce work. A passive device produces the same output which is only dependent on the external input, such as a mass–spring–damper system. A semi-active device is obtained when a control variable is used to change a feature of an element of the system (e.g. a mass–spring–magnetorheological damper where the force exerted by the damper depends on the current). This system anyhow lacks any actuation capacity, it always needs an external stimulus. An active device, such as the MRE actuator, is able to perform work against external forces due to its peculiar design. Ferromagnetic particles embedded in the solid elastomeric matrix [1–3] provide MREs with several advantages over MR fluids, such as the ability to maintain their shape without special sealings. Several researchers have investigated the magneto-mechanical behaviour of MREs and their potential applications in vibration damping, adaptive structures, and semi-active systems. The application of a magnetic field to MREs causes a quick and reversible change in the elastic and loss modulus of the material, which strongly affects its mechanical response. MREs can be controlled as well as MR fluids, as reported in the

Technical Editor: Jovana Jovanova.

✉ Andrea Spaggiari
andrea.spaggiari@unimore.it

[1] Department of Sciences and Methods for Engineering, University of Modena and Reggio Emilia, Reggio, Italy

technical literature [4, 5], but their application as actuators is often limited to research work. Many research groups investigated MREs to describe and model their magneto-mechanical behaviour, considering both static and dynamic loads [6–11]. Typically, these aspects are tackled through refined analytical models of the viscoelastic rubber matrix which holds the ferromagnetic particles and deriving the effect of the magnetic field on the MREs response in terms of viscoelastic parameters (storage modulus, loss modulus [10, 12]) and failure stress [13]. Typical applications include vibration damping [14, 15], adaptive structures [16–18], and semi-active systems that exploit the change in stiffness of the MRE to change the natural frequency of a structure or a system [19]. Recent reviews of MRE applications can be traced in the technical literature [20, 21], but their content mainly considers MRE as passive or adaptive devices. This work would walk another path, though less explored, namely the exploitation of MRE capabilities as actuators, eventually combined with other systems. The research group led by Professor Böse has envisioned some potential applications of MREs for valve actuation [2, 22–24], while embedding MREs in origami structures was a technique proposed by Von Lockette [25]. MREs are semi-active materials so they are not capable of generating work as shape memory alloys, for example; therefore, an easier way to exploit them is to apply them in a sandwich system which couples MREs with CFRP skins [26], thus obtaining a variable stiffness as a function of the magnetic field. While [27] provides a review of MRE sandwich applications and [28] covers a potential application in a patent, a particularly interesting review in the field of MRE actuators is documented in [29], which features several examples of variable stiffness devices. Although the soft actuator proposed by Kashima et al. [30] is a suitable example of an actuator, MREs are generally more challenging to implement in actuator devices than in variable stiffness or shock absorber devices. This is due to the fact that an MRE (or MRF) used in a semi-active way is simpler to design because it can be adapted from an already existing passive design, whereas the use of a MRE in an active way is more challenging because it usually cannot be derived from already existing systems. Thus, this paper aims to explore the feasibility of MREs as a linear actuator by utilizing a commercial magnetic system coupled with a customized MRE disc. The proposed linear actuator is able to provide a force in axial direction similarly to a commercial solenoid, but in addition to that the elastic part of the MRE matrix provides a self-centring force which tends to facilitate the return of the actuator in its central, rest position. The spring force on the disc will always be in the opposite position to the motion, while the magnetic force will always be directed towards the electromagnet (see Figure @4). Moreover, exploiting a flexible element smart like the MRE could integrate both the actuation and the return in one part reducing the system complexity and increasing its robustness.

An innovative actuator like the one described in this work would be interesting to be embedded in a mechanical system because the magnetic actuation could produce work (a force and a stroke) without many moving parts as in traditional mechanical actuators (due to mechanical transmissions, connections, etc.). The MRE, with its ease of casting, could have many advantages, such as being shaped in any form, a disc like in this manuscript or as a dome or in any other geometry. A portion of tube could become an active element if made in MRE, being able to provide the pumping of fluid operator through the piping, as already proposed in [2], or they could be exploited for soft robot grippers as shown in the literature [31–33]. Another application which has an embodiment for the MRE as a disc is also proposed recently by Bernat [34] where the MRE is coupled with a dielectric elastomer to serve as actuator. Moreover, a work from Spaggiari et al. [35] shows how a membrane pump could be obtained through the use of shape memory alloy (SMA) springs; with an MRE actuator like the one presented in this work a similar design could be obtained. Anyhow, for this type of material we envision generally low scale actuators; micro-actuations of a few mm, a few N of force, a dozen Joules at most. These systems cannot be used for large forces or strokes since the magnetic field is exponentially dependent on distance, so moving away from the magnetic source causes a sudden drop in the force. Furthermore, the MRE matrix has a low Young's modulus, so it cannot express large forces even though it could express high local deformations.

MREs have been largely used in the field of vibration damping and in other semi-active systems; moreover, there are few works in the literature that exploit MREs as actuators for active applications. Since MREs present several advantages when embedded in mechanical systems as previously said, in this work is presented a simple MRE actuator based on a commercial electromagnet.

The first section of this paper details the analytical model of the magneto-mechanical system, while the second section outlines the finite element models utilized to validate the design. The last part is devoted to the experimental test and comparison with the models. The actuator manufacturing process and experimental results confirm that the proposed idea is viable, and a simple analytical model may be used as a design tool for such systems.

2 Materials and methods

2.1 Actuator description

This work intends to exploit MREs in a linear actuator by coupling them with a commercial electromagnet with the

aim of providing a certain desired force and/or desired stroke. The design process was driven by the commercial electromagnet chosen, schematically depicted in Fig. 1a, with the core in grey and the coil in light copper. According to the datasheet, this commercial coil (Fig. 1b) has a total power consumption of 8.2 W and is typically used to lock emergency doors [36]. The system is powered at 24 V DC with a nominal current of 340 mA. The turns of the coil are 1750, and the main dimensions are reported in Fig. 1a where $d_i = 35$ mm, $d_o = 65$ mm, $h = 35$ mm, with the custom drilling of a central $d_h = 8$ mm through-hole. Since the actuator is coupled with an MRE, the commercial plate is not needed, but, to achieve the possibility to move both in upward and downward direction a ferromagnetic annular spacer, represented in light purple in Fig. 1a, was added on top of the electromagnetic core. Then, the MRE disc (in yellow in Fig. 1a) was placed onto it. The ferromagnetic spacer and the MRE were tightened on the electromagnet on the annular periphery. With the aim of creating a simple but consistent analytical magneto-mechanical model of the system, we considered the following simplifying hypotheses:

- All the materials have a linear B-H relationship, due to the low field involved;
- Magnetic hysteresis is not considered, since the actuation is DC;
- All flux lines stay inside the magnetic yoke and negligible dispersion occurs in the surrounding air, motivated by the permeability of the materials involved;
- The gap between the magnetic core and the MRE is considered as a constant.

Among these hypotheses, the strongest is the last one, since the gap is clearly varying during the actuation, but we aimed at building a simple model for design purposes and the last hypothesis it is exploited to simplify the procedure. The material hysteresis and the energy loss due to viscoelasticity of the matrix are not considered in the model since the Sylgard 184, according to Zhang et al. [37], shows a quite peculiar insensitivity to the deformation rate and very low elastic hysteresis. Therefore, this simplifying hypothesis seems appropriate for a preliminary design approach of an actuator for low-frequency applications. Future works will investigate the design of similar actuators for dynamic applications, where the viscoelastic contribution will be considered.

It is therefore straightforward to write the area of the MRE where the flux lines pass as:

$$A_{MRE} = \pi d_m t = 2\pi r_m t = 2\pi \frac{r_o + r_i}{2} t = \pi t\left(r_o + r_i\right) \tag{1}$$

where t is the MRE thickness, $r_o = d_o/2$ the electromagnet outer radius and $r_i = d_i/2$ the inner coil radius; d_m is the mean diameter; and r_m is the mean radius between r_o and r_i.

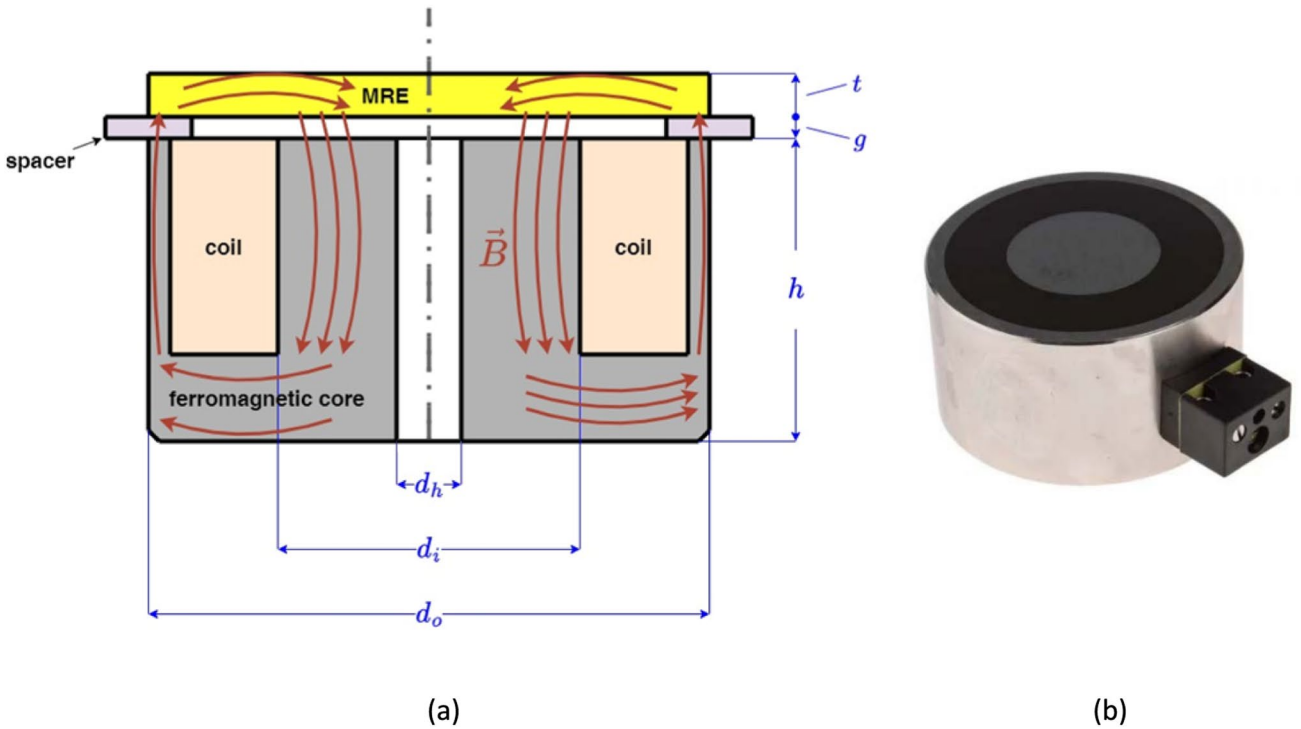

Fig. 1 Schematic of the actuator (**a**) and picture of the commercial electromagnet (**b**) with the custom central through-hole

On the other hand, the area of the air gap where the electromagnetic field passes is:

$$A_{gap} = \pi\left(r_i^2 - \frac{d_h^2}{4}\right) \tag{2}$$

where d_h is the diameter of the central threaded hole of the electromagnet. The reluctance of the system is given by the sum of reluctance of the air gap $\mathcal{R}_{gap}$ due to the spacer and the reluctance of the MRE $\mathcal{R}_{MRE}$ which are computed by using Eqs. (1) and (2).

$$\mathcal{R}_{tot}(g) = \mathcal{R}_{MRE} + \mathcal{R}_{gap} = \frac{r_o - r_i}{\mu_0 \bullet \mu_{MRE} \bullet A_{MRE}} + \frac{g}{\mu_0 \bullet \mu_{air} \bullet A_{gap}} \tag{3}$$

Here, μ_0 is the permeability of free space, μ_{MRE} is the relative permeability of the MRE, and μ_{air} is the relative permeability of air, which can be considered equal to 1. The electromagnet force can be obtained through the partial derivative of the magnetic potential U, where L is the inductance of the coil, a function of the number of turns N and the applied current I.

$$U = \frac{1}{2}LI^2 = \frac{1}{2}\frac{N^2}{\mathcal{R}_{tot}}I^2 \tag{4}$$

The magnetic force therefore is obtained by substituting Eq. (3) in Eq. (4) and deriving the magnetic potential with respect to the gap, g:

$$F = \frac{\partial}{\partial g}U = -\frac{N^2 I^2}{2 \bullet \mu_0 \bullet \mu_{air} \bullet A_{gap} \bullet \mathcal{R}_{tot}^2} \tag{5}$$

This expression helps to understand how the magnetic attraction depends on the gap g and current I. Figure 2a shows the 3D chart used for design purposes, where the force (normalized with respect to its maximum) is depicted as a function of the gap and the applied current. The magnetic force acting on the MRE is assumed to be independent of the radial coordinate and depends only on the initial position of the disc (gap). These assumptions will be verified using a numerical simulation in the next section. It is worth noting that the increasing the spacer height (the gap, g) decreases the available force but provides room for the linear stroke.

One of the aims of the model is to define the optimal trade-off between available force and possible displacement, as it typically happens in many actuators, and to provide the designer with the tool to choose according to the user needs. This is the motivation behind the study of two different air gaps as described in the experimental test description. In order to express the maximum deflection in the centre of the MRE disc, the distributed load q (Fig. 2b) is needed and it can be calculated as the force over the area of the MRE; therefore, according to [38], we have:

$$f = \frac{3qR^4}{16Et^3}\left(1 - \nu^2\right) \tag{6}$$

where E and ν are the elastic modulus and the Poisson ratio of the MRE, respectively.

The two main design variables are g and t, as they have a strong effect on the actuator response and can be easily changed; therefore, we designed a simple experimental plan where two possibilities for each variable are tested, for a total of four different configurations, as described in Fig. 3a.

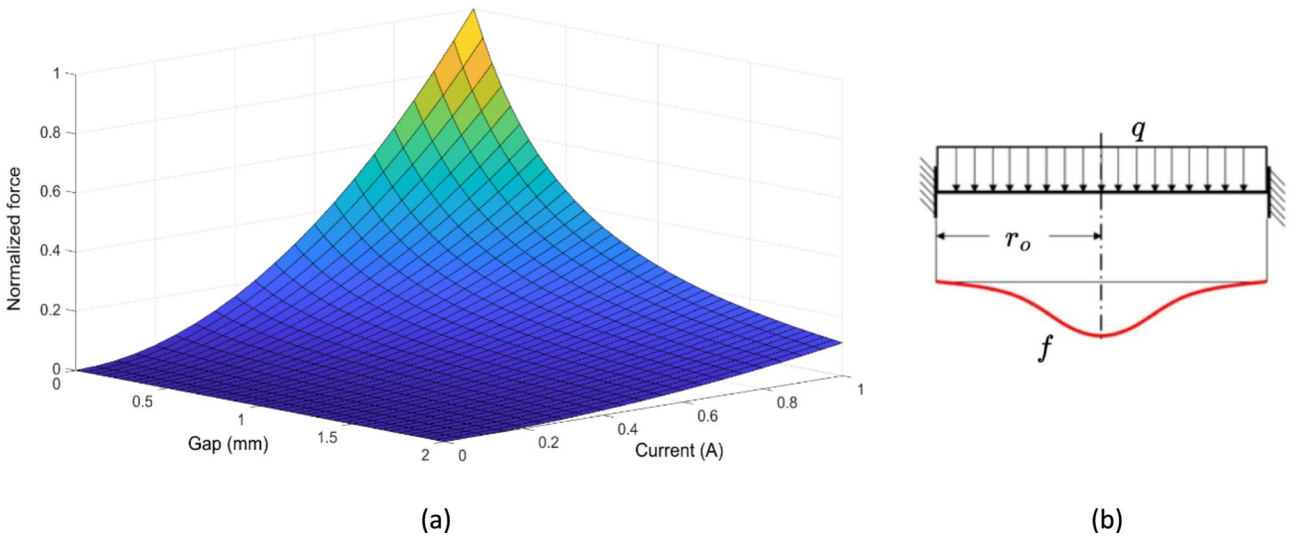

Fig. 2 Response surface of the magnetic force (normalized) as a function of the gap and the current (**a**) and schematic of the MRE disc deflection (**b**)

The MRE was then manufactured as described in [13] with a base elastomer made in Sylgard 184 [39], an RTV silicone already used in many other MRE applications [8, 40–42] with a 30% volume of carbonyl iron particles with an average dimension of 45 µm. More precisely, the manufacturing of the MRE discs consists of four sequential steps:

- manual deposition of the components of the elastomeric matrix (Sylgard 184 and curing agent) inside a specially made ABS mould using a precision scale;
- Addition and mixing of the iron particles in the mould;
- 15 min degassing phase at −0.6Bar (Fig. 3c) to eliminate air in matrix before polymerization;
- polymerization in a climatic chamber (about 4 h at 80 °C).

During the polymerization phase, the mould is closed and mounted on a rotating platform driven by a stepper motor so that the iron particles do not settle down during the curing process. Therefore, the MRE discs obtained will have a random isotropic arrangement of iron particles within the elastomeric matrix. Future works will consider also

	gap (mm)	MRE thickness (mm)
t4g2	2	4
t4g4	4	4
t6g2	2	6
t6g4	4	6

(a)

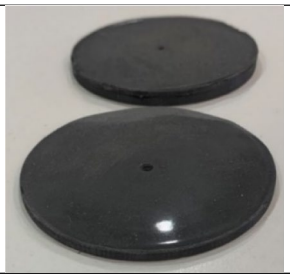

(b)

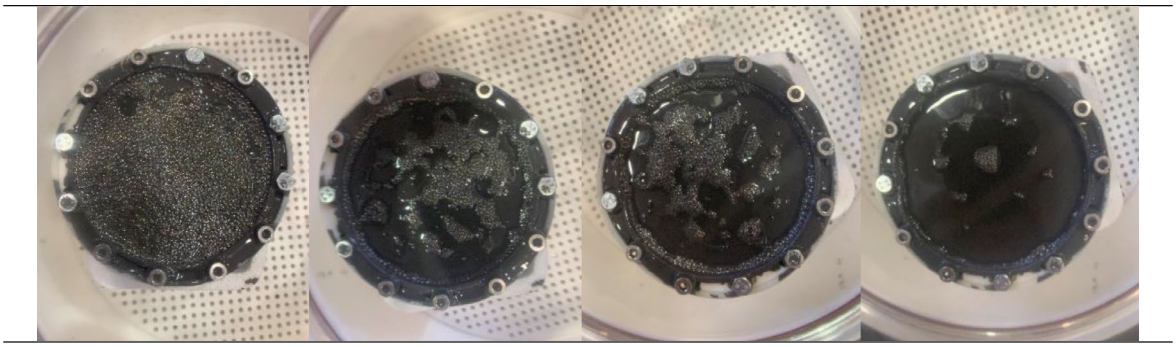

(c)

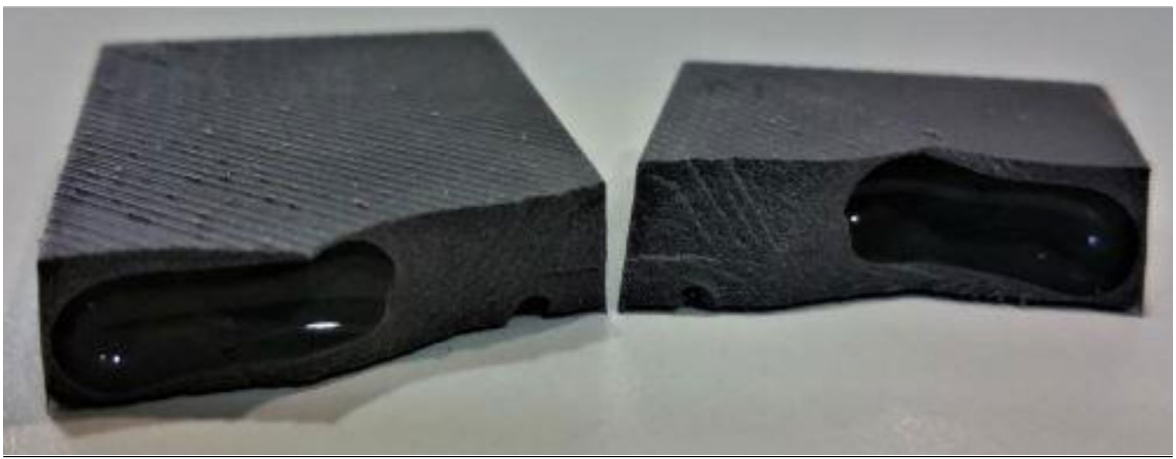

(d)

Fig. 3 Combination of experimental variables considered in the actuator design (**a**), an example of MRE discs used in the actuator (**b**), the degassing phase during the manufacturing of the discs (**c**), and sections of a polymerized MRE with air bubbles in its matrix (**d**), showing the importance of a correct degassing phase before polymerization [8]

anisotropic disc with particle aligned in columns to evaluate the response of the actuator with a non-random particle distribution. According to previous literature work [8], the 30% volume concentration of particles is optimal to achieve good magneto-mechanical properties such as an elastic modulus of 3 MPa, a Poisson ratio of 0.49, as for many elastomers it is nearly incompressible [43], and a relative magnetic permeability of,$\mu_{MRE} = 4$, which is assumed to be linear for simulation purposes due to the low magnetic field [44]. A sample of the MRE disc is reported in Fig. 3b, where a very small hole was added in the centre to hold the connector to the load cell. A central rigid pin is used in the experiment test to this extent. Although the presence of the central hole and the pin modifies the constraints conditions of the MRE membrane, it is still possible to apply an analytical formula to obtain the force deflection relationship, as reported in Roark et al. [38]. A Galdabini SUN 500 testing machine equipped with a 250 N load cell was used to perform the experimental tests.

The experimental tests were designed to find out the force–stroke characteristic of the actuator. In particular, they were carried out applying first a 3 mm upward displacement through the central pin (Fig. 4a). The system was then released, and the machine crosshead was set to − 1.5 mm, which is the maximum downward stroke, in the lowest gap configuration. Finally, the system returns to zero. This cycle is shown in Fig. 4b and was used with currents ranging from 0 up to 800 mA. The elastic force of the MRE always opposes crosshead movement, while the magnetic force always pulls in the downward direction. This peculiarity of the proposed actuator provides an unusual force–displacement characteristic, which is more challenging for the model to follow. The complete experimental rig is shown in Fig. 4c.

2.2 Finite element models

2.2.1 Magnetic numerical model

The analytical predictions are based on strong hypotheses which needs to be verified; therefore, a numerical model was implemented to compare the results. A magnetostatic finite element software, FEMM [45], was used to estimate the magnetic induction field that insists on the MRE. It was possible to exploit the axial symmetry according to the

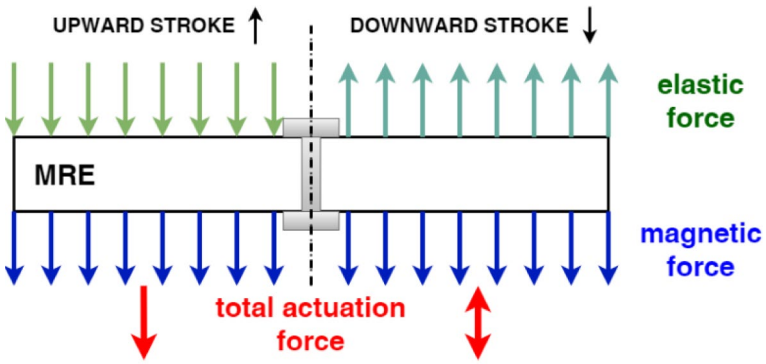

(b)

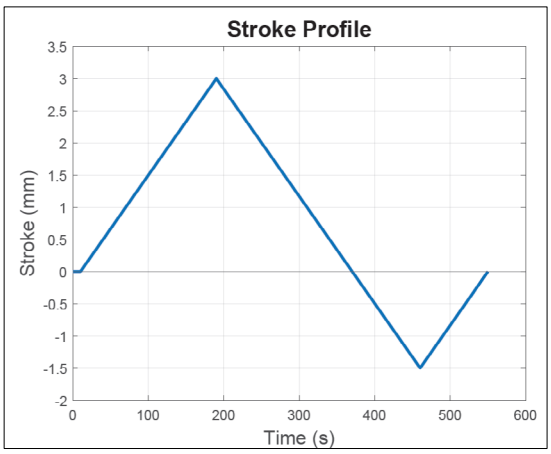

(a)

(c)

Fig. 4 Experimental stroke profile for the tests (**a**), forces on the cursor (**b**), and experimental set up (**c**) where the rigid pin is highlighted in white (colour figure online)

system geometry. The materials of the electromagnet were modelled as reported in the electromagnet datasheet, while the MRE disc is considered linear, with the $\mu_{MRE} = 4$, as in the analytical model, while the spacer (made of ferritic stainless steel AISI 430) was modelled with a relative magnetic permeability of 800 [46]. From this model, the analytical prediction in terms of magnetic field inside the MRE and attraction force can be assessed, and the outcome will be presented in the results section. Figure 5a shows the mesh with refinements at the discontinuity in a particular configuration (t6g4), but the four cases were analysed to increase current values, ranging from 200 up to 800 mA applied for 10 s. The electromagnet datasheet provides a nominal current of 340 mA as the limit for continuous use due to thermal considerations, but it is possible to inject an overcurrent of up to 800 mA for a short time to obtain a higher magnetic field, a larger force on the MRE with almost no overheating of the system. Mechanical numerical model.

The analytical predictions, especially the deflection, are assessed by means of finite element model as shown in Fig. 5b. We developed a simple axially symmetric model made using the *Simulation* tools of SolidWorks with constraints on the periphery of the MRE disc, just like in the physical actuator. The analysis is geometrically nonlinear and relies on the elastic properties of the MRE mentioned in the previous section. The applied load is obtained from the previous FEMM analyses described in Sect. 2.2.1. The output of this model is the deflection at the centre of the MRE disc, which will be compared both with the analytical prediction and with the experimental data in the Results and Discussion section.

3 Results and discussion

3.1 Numerical results

3.1.1 Finite element magnetic simulation results

Figure 6 shows the results of the magnetic simulations for the four configurations considered with a nominal current of 500 mA. The main output of these analyses is the forces exerted on the MRE element by the electromagnet, as shown in Table 1. The analysis exploits the axial symmetry of the system; therefore, only half of the model is shown in Fig. 6. The computation of the magnetic force, reported in Table 1, already considers the integral over the entire area of the MRE disc.

3.1.2 Finite element mechanical simulation results

The results of the finite element simulations carried out on the MRE membrane as depicted in Fig. 7 show the deformation of the MRE under the forces computed by the FEMM simulations. Figure 7 represents the axial displacement for the four configurations with the same nominal current of 500 mA.

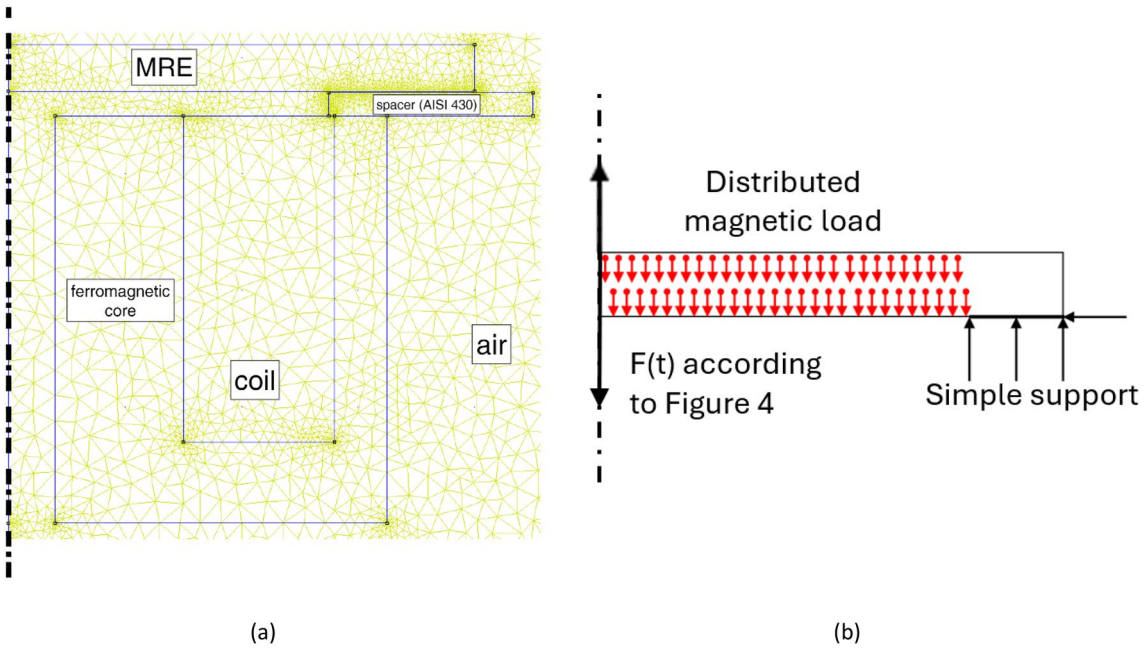

Fig. 5 FEMM magnetic model (**a**) and axisymmetric finite element model with distributed load taken from the FEMM simulation and constraints consistent with the prototype (**b**)

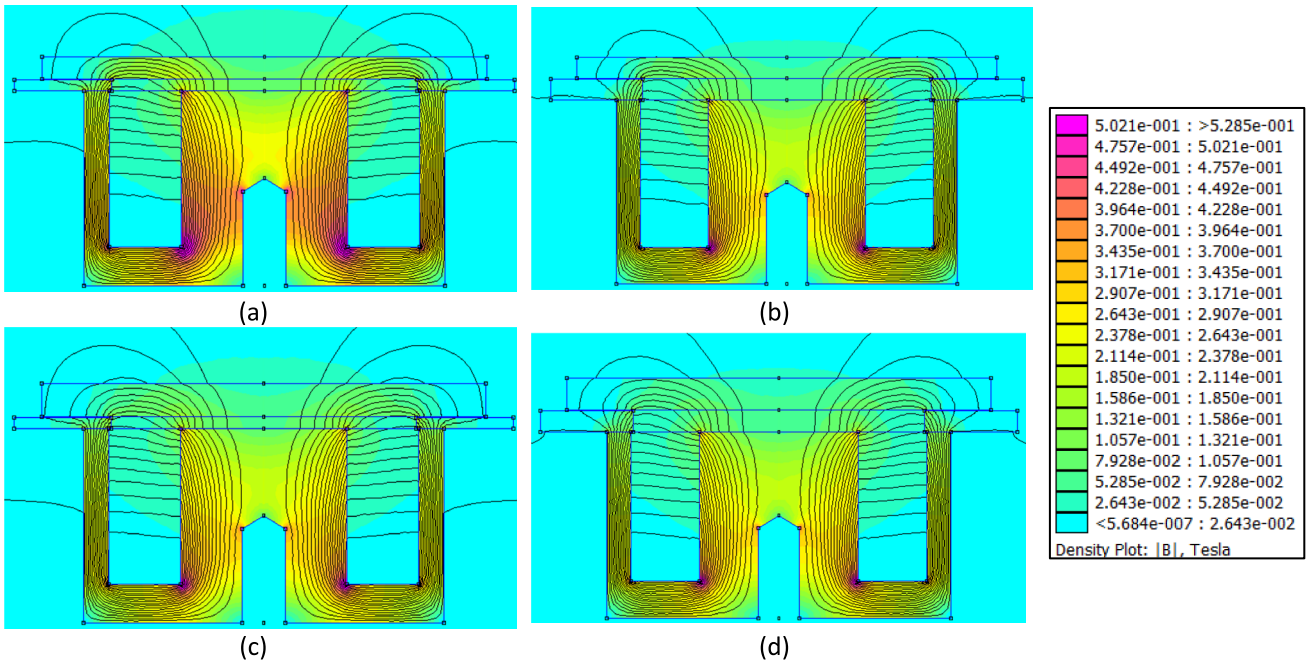

Fig. 6 Magnetic FEMM simulations at 500 mA for t4g2 (**a**), t4g4 (**b**), t6g2 (**c**), and t6g4 (**d**), and a density plot of the induction flux (T) for t4g2 configuration

Table 1 Numerical magnetic force obtained by simulations (integral on the entire area of the MRE disc)

I (mA)	Force (N)			
	t4g2	t4g4	t6g2	t6g4
100	0,38	0,23	0,48	0,28
200	1,53	0,90	1,93	1,10
300	3,45	2,05	4,33	2,48
400	6,13	3,64	7,70	4,42
500	9,58	5,69	12,02	6,90
600	13,78	8,19	17,29	9,92
700	18,71	11,13	23,46	13,48
800	24,35	14,50	30,52	17,56

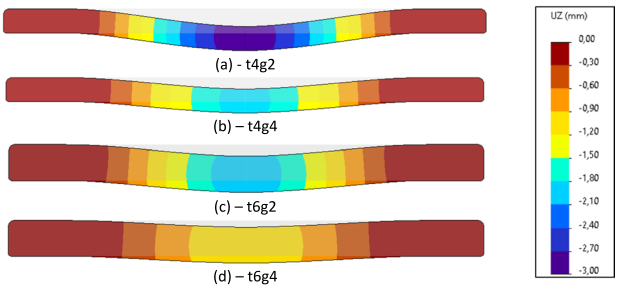

Fig. 7 FEM results: axial displacement of the MRE disc at 0.5 A for t4g2 (**a**), t4g4 (**b**), t6g2 (**c**), and t6g4 (**d**), superimposed to the unloaded configuration

The main purpose of the finite element analysis was to validate the simple analytical model of the actuator proposed in Sect. 2.1. As can be seen in Fig. 9, the numerical results obtained through FEMM reflect the proposed analytical model very well. Furthermore, in the same figure it can be seen how the numerical analyses and the analytical model slightly underestimate the force expressed by the actuator at the various current levels. This difference is due to the simplifying assumptions applied to the analytical model. This minor underestimate is anyhow conservative, since the actuator will exert at least the desired force, as shown in the Experimental results section (Table 2).

3.2 Experimental results

The experimental tests are reported in Fig. 8 for the four combinations of gaps and MRE thicknesses and applied currents. As expected, the force increases with increasing current, and also depending on the stroke, as the MRE disc acts as a spring. The force at zero stroke, when the crosshead is blocked, can be interpreted as the net magnetic contribution. When the experimental stroke profile shown in Fig. 4a is applied, the force first increases, then decreases, and finally returns to its starting values. It should be noted that the stroke is not symmetric, as there are no limitations on the upper stroke allowing the disc to be pulled up to 3 mm, while the stroke in the lower direction (shown as negative

in Fig. 8) is limited by the gap, and fixed at − 1.5 mm, to prevent the MRE disc from hitting the electromagnet.

Focusing on the forces at zero stroke, it is possible to compare the analytical prediction of the model given by Eq. (6) and the numerical value obtained by the FEMM simulation. A comparison is provided in Fig. 9, where it is seen that the numerical and analytical predictions are in good agreement, while the experimental predictions are always higher in terms of force, especially at high currents. The reason is that the model does not consider the gap reduction resulting from disc movement and the subsequent increase in the magnetic force. Nonetheless, since the analytical model provides a lower force prediction, it can be safely used for design purposes, and the real application will provide at least the desired force. As can be seen, the best performance in terms of force is given by a large thickness (6 mm) and a low gap (2 mm). It is worth noting that lowering the gap has the drawback of lowering the stroke, so a trade-off between the two variables should be found according to the needs of the designer.

3.3 Discussion

The actuator response is characterized by two main components, the controllable one, i.e. the force due to the magnetic field and the elastic component, which is always present irrespective of the field. Therefore, it is interesting to provide an estimate of the controllable force separately, in order to assess the dynamic range [47–50]. The dynamic range is a figure of merit that is commonly used in MR devices and is defined as the total force over the uncontrollable forces. The latter can be defined as all the force except the pure magnetic one; therefore, there is the need to estimate the pure magnetic force component, for which the following procedure is adopted. We tested all four configurations with no magnetic field applied following Fig. 4 profile and subtracted from the curves reported in Fig. 8 these results, thus obtaining the pure magnetic force curves as a function of the displacement. The curves obtained are reported in Fig. 10, where the four geometries are considered. The first thing that can be noticed is that the curves present an almost linear behaviour in general, with two notable exceptions, i.e. the curve at 800 mA where there is a lower magnetic force in case of negative stroke. This unexpected phenomenon could be ascribed to the magnetic saturation which could occur when the MRE is very close to the electromagnet.

This phenomenon is also confirmed by the raw experimental data in Fig. 8c and d, where at negative strokes the 800 mA curve for the 6 mm MRE discs is almost superimposed on the 600 mA ones. To have a simpler measure of

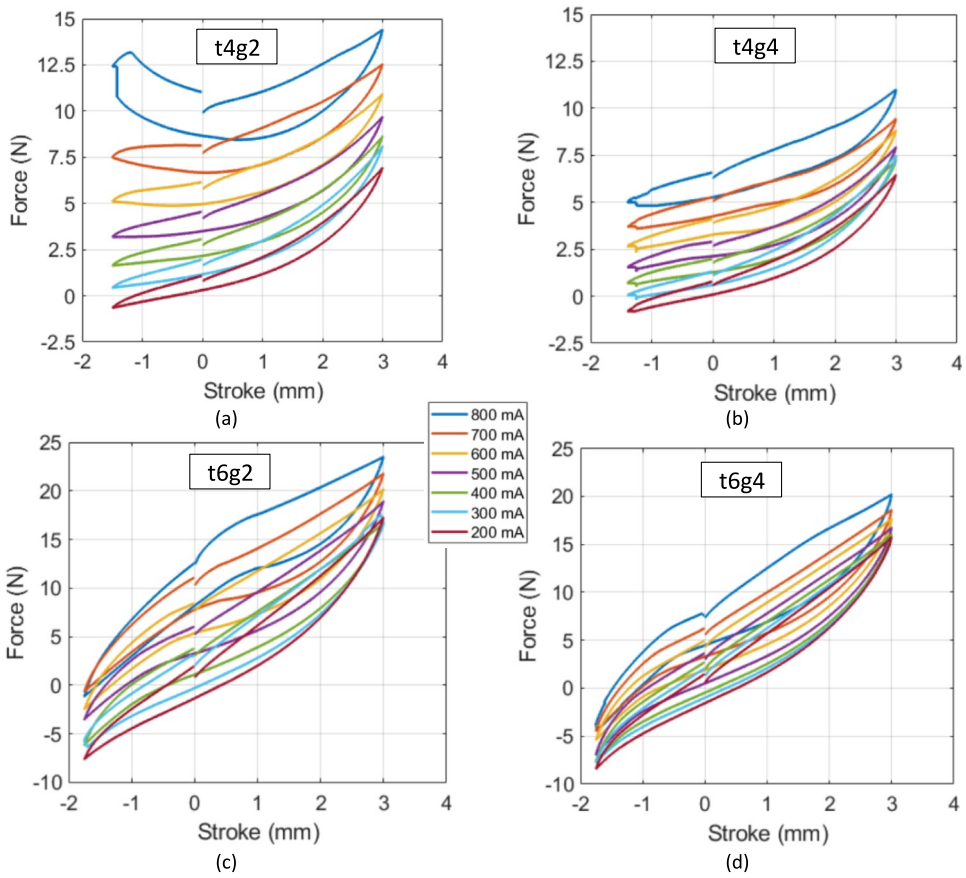

Fig. 8 Experimental force–displacement curves for the four configurations considered, under the displacement profile applied and for currents ranging from 200 to 800 mA. Thickness 4, gap 2 (**a**), thickness 4, gap 4 (**b**), thickness 6, gap 2 (**c**), and thickness 6 gap 4 (**d**)

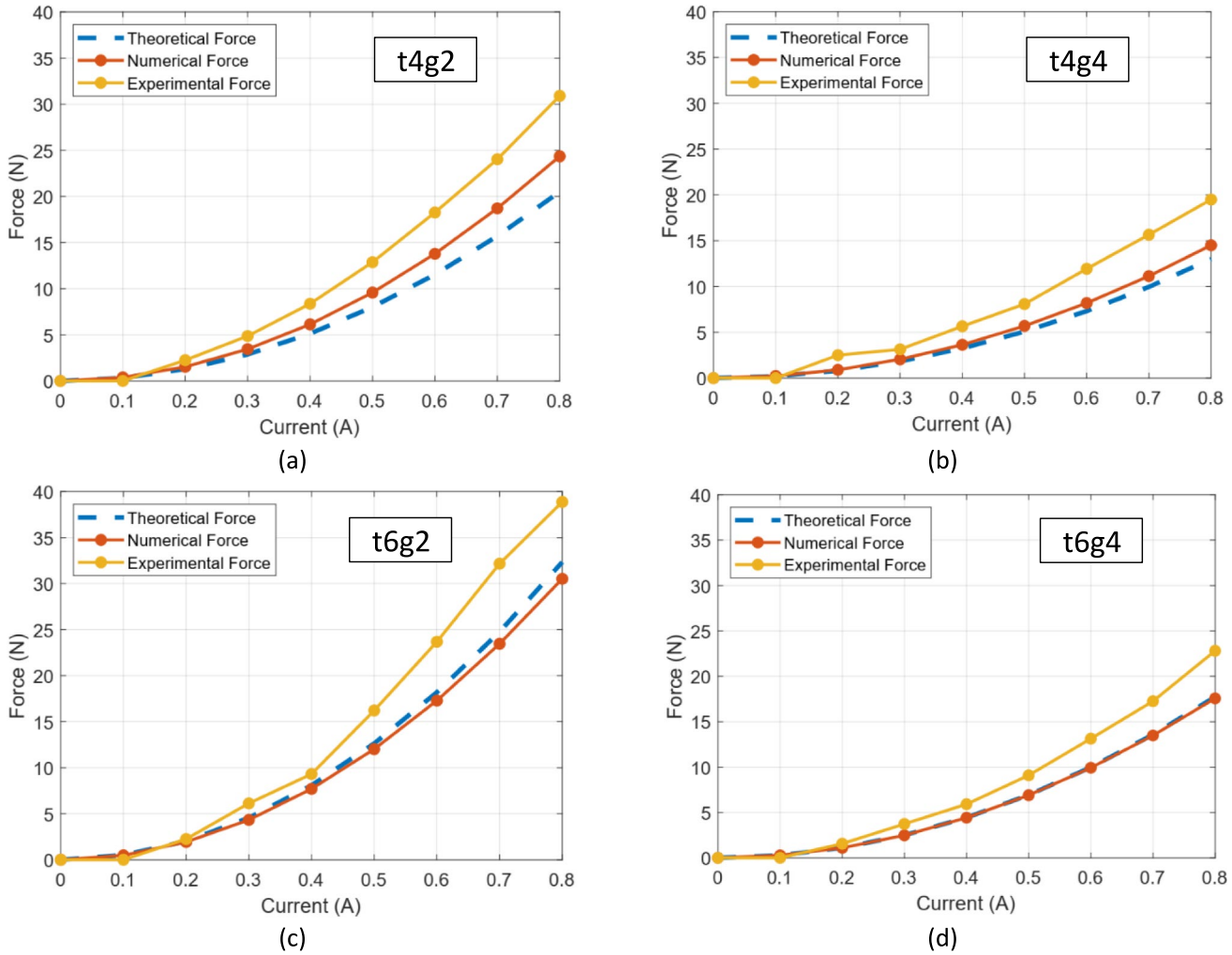

Fig. 9 Comparison between experimental force at zero displacement for the four configurations considered, for currents ranging from 200 to 800 mA. Thickness 4, gap 2 (**a**), thickness 4, gap 4 (**b**), thickness 6, gap 2 (**c**), and thickness 6, gap 4 (**d**)

the pure magnetic force and therefore estimate the dynamic range across the entire stroke, it is possible to interpolate these data and build a response surface. The fitting of the curve is carried out with an optimization procedure in MATLAB, and the best fitting is obtained with a linear polynomial law with the deflection, f, and quadratic with the current, I, which is consistent with Eq. (5).

The pure magnetic force, F_m, is therefore reported in Eq. (7), with the coefficients as in the table below:

$$F_m = \alpha \mathrm{I} + \beta \mathrm{f} + \gamma \mathrm{I}^2 + \delta \mathrm{fI} \tag{7}$$

The response surface generated by these interpolations is reported in Fig. 11 and compared with the experimental data. This chart provides useful information about the influence of the geometry on the pure magnetic force, thus helping the designer increase the dynamic range. Figure 11a shows the influence of the gap at the same thickness (4 mm). The lower gap (2 mm) is able to provide a larger magnetic force, nearly 50% more than the higher one at 800 mA. The increment is lower when the MRE thickness is larger; as in Fig. 11b, only a 20% increase is visible for the 2 mm gap and the 10% in the 4 mm gap.

The dynamic range, obtained by computing the maximum experimental points of the curves in Fig. 9 and the pure magnetic forces of Fig. 10 at zero displacement, is quite stable, and it is around 1.5 for every configuration, for the maximum current of 800 mA. This means that irrespective of the total force exerted by the actuator, which can be seen as the size of the system, the increment provided by the magnetorheological controllable parts produces an increment of the force around + 50% for all configurations. (b).

The proposed MRE actuator can produce work only when the electromagnet is active and the MRE moves in the negative direction, but due to its elastic component, it is also capable of withstand movement in the opposite

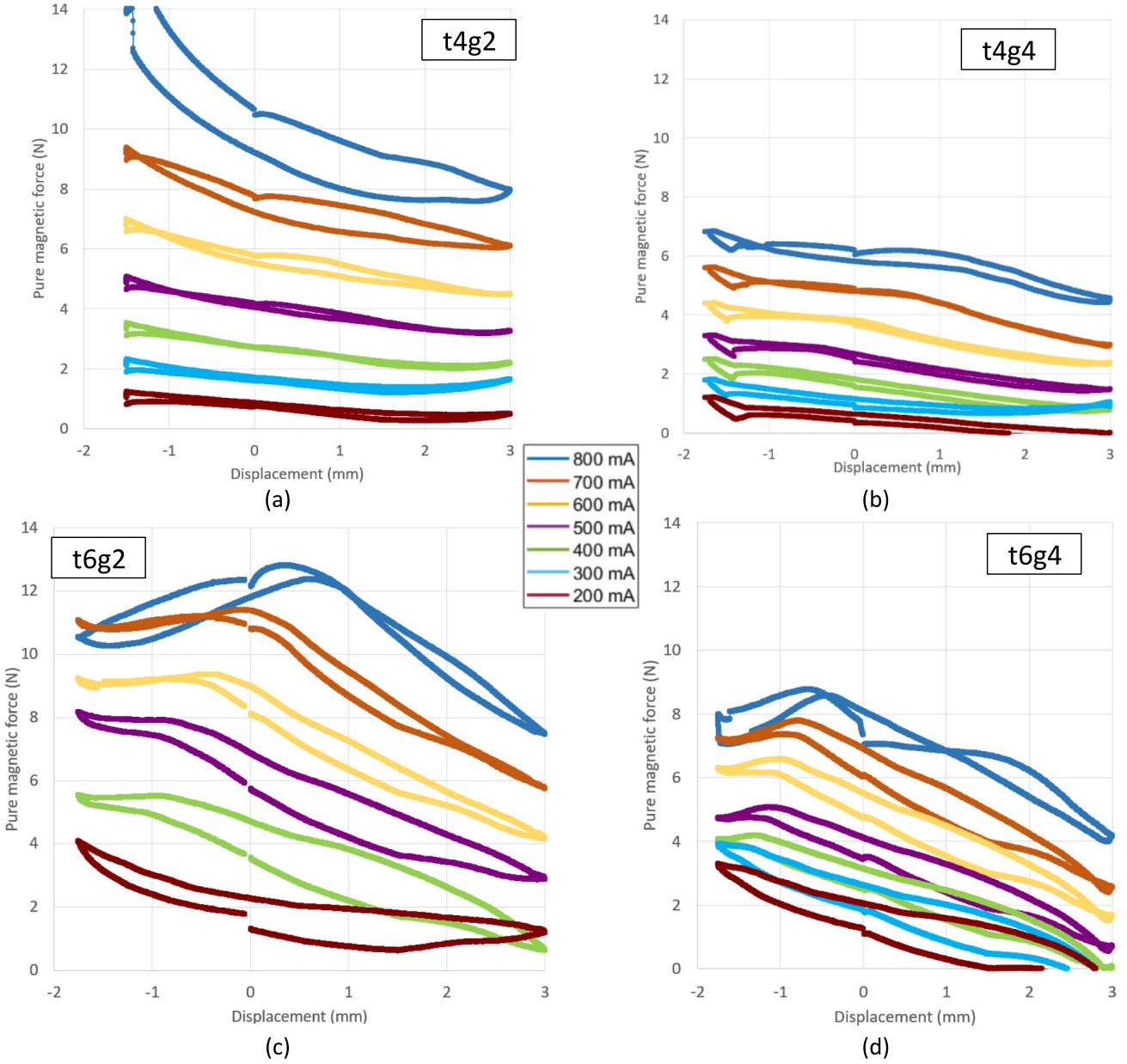

Fig. 10 Pure magnetic force obtained from experimental curves, for currents ranging from 200 to 800 mA. Thickness 4, gap 2 (**a**), thickness 4, gap 4 (**b**), thickness 6, gap 2 (**c**), and thickness 6, gap 4 (**d**)

Table 2 Coefficient of the best fitting of the numerical force as a function of the geometry

	t4g2	t4g4	t6g2	t6g4
α	1.2031	1.0276	6.9364	5.0998
β	0.029	−0.1035	−0.357	−0.5577
γ	14.1765	8.1529	10.5643	5.3306
δ	−0.8763	−0.5566	−1.3748	−0.6937

direction, although with lower forces. A flexible actuator can be exploited in many applications and, thanks to the simple analytical formulae provided, can be designed according to the specific needs. A work from Xu et al. [51], for example, shows how MREs could be used to design flexible robotic grippers providing forces comparable to the ones exerted by the actuator presented here.

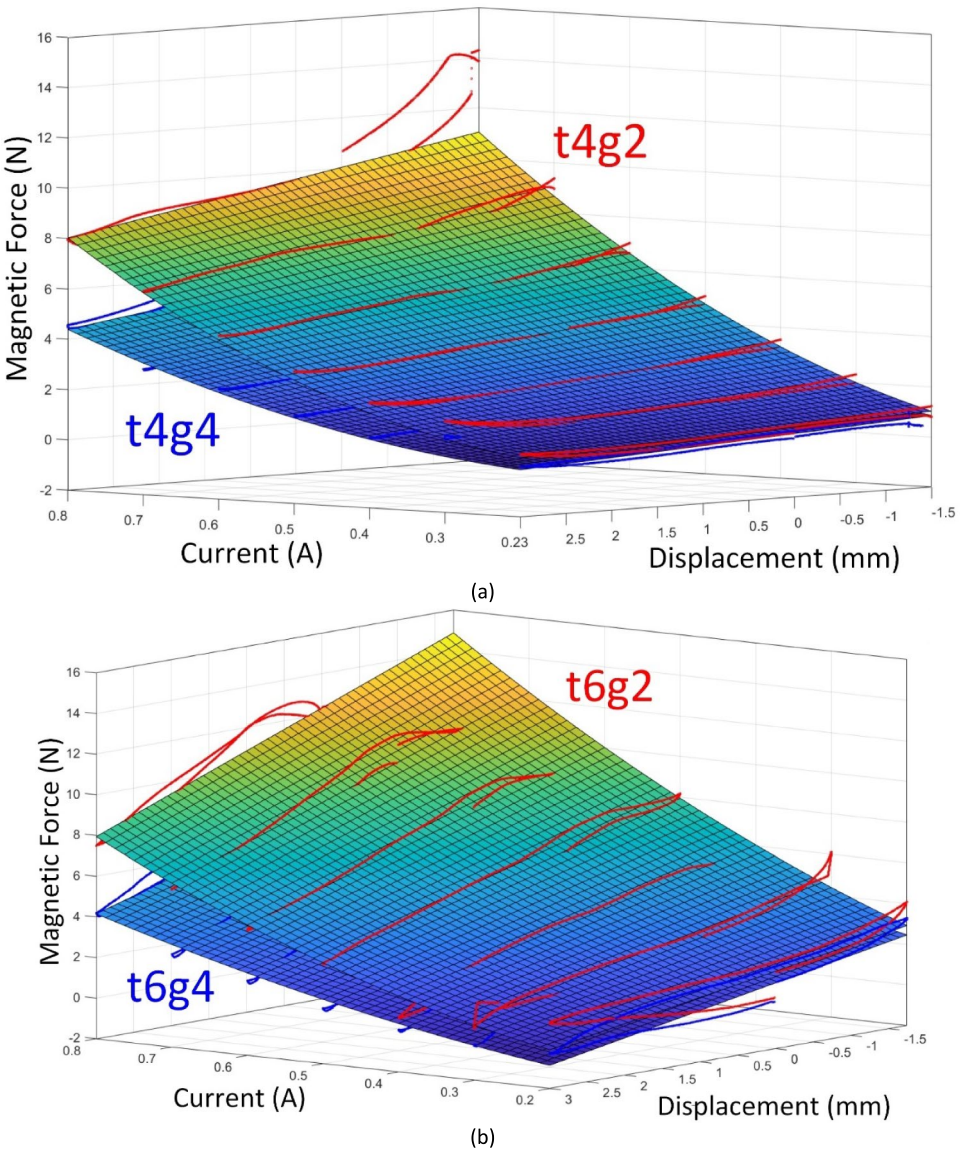

Fig. 11 Response surface for 4 mm thickness (**a**) with experimental data in red and in (**b**) for 6 mm thickness for the tested values of current and displacement

4 Conclusion

This research study focuses on the design and characterization of an innovative actuator which exploits a disc in magnetorheological elastomer coupled with an electromagnet. The study includes the development of a simple yet informative analytical model to assess the feasibility of the system, extensive mechanical and magnetic finite element simulations to refine the design, prototyping and testing of the actuator and collection of the experimental results in terms of force displacement behaviour of the system. This particular embodiment of an MRE actuator has potential applications in engineering system where strong integration and low forces are involved, especially where there is the need of have almost no moving parts. The actuator consists of a commercial electromagnet, a MRE disc, and a supporting frame. Four different configurations of the system are analysed by considering two possible disc thicknesses and two gaps between the elements, and the accuracy of the analytical and numerical models is checked against the experimental results. The study correlates the force response with actuator morphology and the current applied to the electromagnet. The experimental results confirm the good agreement between the analytical and numerical models, with the analytical model which underestimates of the force exerted by the prototype of actuator. A model of the pure magnetic force is provided in order to estimate the contribution of the controllable part against the total force to assess the dynamic range. The study concludes that this MRE-based linear actuator design, which has the peculiar feature of being adaptable to many applications and shapes since the MRE part can be casted in almost every shape, is feasible and that the analytical model can be exploited for design purposes.

Funding Open access funding provided by Università degli Studi di Modena e Reggio Emilia within the CRUI-CARE Agreement.

Data availability Data will be available upon request.

Declarations

Conflict of interest The authors declare that there are no conflicts of interest.

References

1. Jaafar MF, Mustapha F, Mustapha M (2021) Review of current research progress related to magnetorheological elastomer material. J Market Res 15:5010–5045. https://doi.org/10.1016/j.jmrt.2021.10.058
2. Böse H, Gerlach T, Ehrlich J (2021) Magnetorheological elastomers — An underestimated class of soft actuator materials. J Intell Mater Syst Struct 32:1550–1564. https://doi.org/10.1177/1045389X21990888
3. Jolly MR, Carlson JD, Muñoz BC (1996) A model of the behaviour of magnetorheological materials. Smart Mater Struct 5:607–614. https://doi.org/10.1088/0964-1726/5/5/009
4. Böse H, Röder R (2009) Magnetorheological elastomers with high variability of their mechanical properties. J Phys Conf Ser 149:012090. https://doi.org/10.1088/1742-6596/149/1/012090
5. Lerner AA, Cunefare KA (2008) Performance of MRE-based vibration absorbers. J Intell Mater Syst Struct 19:551–563. https://doi.org/10.1177/1045389X07077850
6. Davis LC (1999) Model of magnetorheological elastomers. J Appl Phys 85:3348–3351. https://doi.org/10.1063/1.369682
7. Tao Y, Rui X, Yang F, Chen G, Bian L, Zhu W, Wei M (2018) Design and experimental research of a magnetorheological elastomer isolator working in squeeze/elongation–shear mode. J Intell Mater Syst Struct 29:1418–1429. https://doi.org/10.1177/1045389X17740436
8. Bellelli A, Spaggiari A (2019) Magneto-mechanical characterization of magnetorheological elastomers. J Intell Mater Syst Struct 30:2534–2543. https://doi.org/10.1177/1045389X19828828
9. Popp KM, Zhang XZ, Li WH, Kosasih PB (2009) MRE properties under shear and squeeze modes and applications. J Phys Conf Ser 149:012095. https://doi.org/10.1088/1742-6596/149/1/012095
10. Kukla M, Górecki J, Malujda I, Talaśka K, Tarkowski P (2017) The determination of mechanical properties of magnetorheological elastomers (MREs). Proc Eng 117:324–330. https://doi.org/10.1016/j.proeng.2017.02.233
11. Schubert G, Harrison P (2015) Large-strain behaviour of magnetorheological elastomers tested under uniaxial compression and tension, and pure shear deformations. Polym Test 42:122–134. https://doi.org/10.1016/j.polymertesting.2015.01.008
12. M. Kallio (2005) The elastic and damping properties of magnetorheological elastomers, http://www.vtt.fi/inf/pdf/.
13. Spaggiari A, Bellelli A (2021) Magnetorheological elastomers characterization under shear loading up to failure: a magneto-mechanical multivariate analysis. J Intell Mater Syst Struct 32:943–954. https://doi.org/10.1177/1045389X20963169
14. Collette C, Kroll G, Saive G, Guillemier V, Avraam M, Preumont A (2009) Isolation and damping properties of magnetorheologic elastomers. J Phys Conf Ser 149:012091. https://doi.org/10.1088/1742-6596/149/1/012091
15. Bastola AK, Li L (2018) A new type of vibration isolator based on magnetorheological elastomer. Mater Des 157:431–436. https://doi.org/10.1016/j.matdes.2018.08.009
16. Eem SH, Koo JH, Jung HJ (2019) Feasibility study of an adaptive mount system based on magnetorheological elastomer using real-time hybrid simulation. J Intell Mater Syst Struct 30:701–707. https://doi.org/10.1177/1045389X18754347
17. Li Y, Li J, Tian T, Li W (2014) Corrigendum: a highly adjustable magnetorheological elastomer base isolator for applications of real-time adaptive control (Smart Materials and Structures (2013) 22 (095020)). Smart Mater Struct 23:129501. https://doi.org/10.1088/0964-1726/23/12/129501
18. Vatandoost H, Hemmatian M, Sedaghati R, Rakheja S (2020) Dynamic characterization of isotropic and anisotropic magnetorheological elastomers in the oscillatory squeeze mode superimposed on large static pre-strain. Compos B Eng 182:107648. https://doi.org/10.1016/j.compositesb.2019.107648
19. Ciocanel C, Nguyen T, Elahinia M (2008) Design and modeling of a mixed mode magnetorheological (MR) fluid mount. Act Passive Smart Struct Int Syst. https://doi.org/10.1117/12.775993
20. Bastola AK, Hossain M (2020) A review on magneto-mechanical characterizations of magnetorheological elastomers. Compos B Eng 200:108348. https://doi.org/10.1016/j.compositesb.2020.108348
21. Samal S, Škodová M, Abate L, Blanco I (2020) Magneto-rheological elastomer composites. A review. Appl Sci 10(14):4899. https://doi.org/10.3390/app10144899
22. Böse H, Rabindranath R, Ehrlich J (2012) Soft magnetorheological elastomers as new actuators for valves. J Intell Mater Syst Struct 23:989–994. https://doi.org/10.1177/1045389X11433498
23. Cruz M, Kyung KU, Shea H, Bose H, Graz I (2018) Applications of smart materials to haptics. IEEE Trans Haptics 11:2–4. https://doi.org/10.1109/TOH.2018.2809058
24. Bose H, Ehrlich J, Gerlach T (2022) Magnetorheological elastomers-material properties and actuation capabilities. IEEE Trans Magn 58:5. https://doi.org/10.1109/TMAG.2021.3081016
25. Bowen L, Springsteen K, Feldstein H, Frecker M, Simpson TW, von Lockette P (2015) Development and validation of a dynamic model of magneto-active elastomer actuation of the origami waterbomb base. J Mech Robot 7:011010. https://doi.org/10.1115/1.4029290
26. de Souza F, Eloy GF, Gomes AC, Ancelotti SS, da Cunha A, Bombard JF, Junqueira DM (2019) A numerical-experimental dynamic analysis of composite sandwich beam with magnetorheological elastomer honeycomb core. Compos Struct 209:242–257. https://doi.org/10.1016/j.compstruct.2018.10.041
27. Sharif U, Sun B, Hussain S, Ibrahim DS, Adewale OO, Ashraf S, Bashir F (2021) Dynamic behavior of sandwich structures with magnetorheological elastomer: a review. Materials 14:7025. https://doi.org/10.3390/ma14227025
28. P. Galitz, T. Heier, C. Schubert, BAYERISCHE MOTOREN WERKE AKTIENGESELLSCHAFT, Actuator having a magnetorheological elastomer element, WO 2010/054775 A1, 2010.

29. Li Y, Li J, Li W, Du H (2014) A state-of-the-art review on magnetorheological elastomer devices. Smart Mater Struct 23:123001. https://doi.org/10.1088/0964-1726/23/12/123001
30. Kashima S, Miyasaka F, Hirata K (2012) Novel soft actuator using magnetorheological elastomer. IEEE Trans Magn 48:1649–1652. https://doi.org/10.1109/TMAG.2011.2173669
31. Choi YT, Hartzell CM, Leps T, Wereley NM (2017) Gripping characteristics of an electromagnetically activated magnetorheological fluid-based gripper. AIP Adv 8:056701. https://doi.org/10.1063/1.5006094
32. Nishida T, Okatani Y, Tadakuma K (2016) Development of universal robot gripper using MRα fluid. Int J Humanoid Rob 13:1650017. https://doi.org/10.1142/S0219843616500171
33. Hartzell CM, Choi YT, Wereley NM, Leps TJG (2019) Performance of a magnetorheological fluid-based robotic end effector. Smart Mater Struct 28:035030. https://doi.org/10.1088/1361-665X/aafe2b
34. Bernat J, Kołota J, Gajewski P, Marcinkowska A (2023) Dielectric elastomer actuator biased by magnetorheological elastomer with permanent magnet. Smart Mater Struct 32:095029. https://doi.org/10.1088/1361-665X/aceddd
35. Spaggiari A, Spinella I, Dragoni E (2012) Design equations for binary shape memory actuators under arbitrary external forces. J Intell Mater Syst Struct 24:682–694. https://doi.org/10.1177/1045389X12444491
36. RS PRO (2024) Access control door magnet - 1670 N holding force, 24V DC, (n.d.). https://uk.rs-online.com/web/c/security-ironmongery/security-alarms-sensors/magnetic-door-locks/ (accessed June 10, 2024).
37. Zhang S, Ge C, Liu R (2022) Mechanical characterization of the stress-strain behavior of the polydimethylsiloxane (PDMS) substate of wearable strain sensors under uniaxial loading conditions. Sens Actuators A Phys 341:113580. https://doi.org/10.1016/j.sna.2022.113580
38. R.J. (Raymond J. Roark, W.C. (Warren C. Young, R.G. (Richard G. Budynas, Roark's formulas for stress and strain, McGraw-Hill, 2002.
39. Dow, SYLGARDTM 184 Silicone Elastomer Kit | Dow Inc., (n.d.). https://www.dow.com/en-us/pdp.sylgard-184-silicone-elastomer-kit.01064291z.html#overview (accessed June 10, 2024).
40. Günther D, Borin DY, Günther S, Odenbach S (2012) X-ray micro-tomographic characterization of field-structured magnetorheological elastomers. Smart Mater Struct 21:015005. https://doi.org/10.1088/0964-1726/21/1/015005
41. Forster E, Mayer M, Rabindranath R, Böse H, Schlunck G, Monkman GJ, Shamonin M (2013) Patterning of ultrasoft, agglutinative magnetorheological elastomers. J Appl Polym Sci 128:2508–2515. https://doi.org/10.1002/app.38500
42. Li WH, Nakano M (2013) Fabrication and characterization of PDMS based magnetorheological elastomers. Smart Mater Struct 22:055035. https://doi.org/10.1088/0964-1726/22/5/055035
43. Müller A, Wapler MC, Wallrabe U (2019) A quick and accurate method to determine the Poisson's ratio and the coefficient of thermal expansion of PDMS. Soft Matter 15:779–784. https://doi.org/10.1039/C8SM02105H
44. Vatandoost H, Sedaghati R, Rakheja S (2022) A novel methodology for accurate estimation of magnetic permeability of magnetorheological elastomers. J Magn Magn Mater 560:169669. https://doi.org/10.1016/J.JMMM.2022.169669
45. D.C. Meeker, Finite Element Method Magnetics, Version 4.2 (28Feb2018 Build), (n.d.). https://www.femm.info (accessed June 11, 2024).
46. Hamilton Precision Metals, Stainless Steel 430, (n.d.). https://www.hpmetals.com/-/media/ametekhpmetals/files/technical-data/stainless-steel/ss%20430.pdf (accessed June 10, 2024).
47. Golinelli N, Spaggiari A (2017) Experimental validation of a novel magnetorheological damper with an internal pressure control. J Intell Mater Syst Struct 28:2489–2499. https://doi.org/10.1177/1045389X17689932
48. Mao M, Wei Hu, Choi Y-T, Wereley NM (2007) A magnetorheological damper with bifold valves for shock and vibration mitigation. J Intell Mater Syst Struct 18(12):1227–1232. https://doi.org/10.1177/1045389X07083131
49. Nie SL, Xin DK, Ji H, Yin FL (2019) Optimization and performance analysis of magnetorheological fluid damper considering different piston configurations. J Intell Mater Syst Struct 30:764–777. https://doi.org/10.1177/1045389X19828526
50. G. Yang, B.F. Spencer, Large-scale magnetorheological fluid damper for vibration mitigation: modeling, testing and control, Ph.D dissertation, University of Notre Dame, 2001.
51. Xu M, Liu Y, Li J, Xu F, Huang X, Yue X (2024) Review of flexible robotic grippers, with a focus on grippers based on magnetorheological materials. Materials 17(19):4858. https://doi.org/10.3390/ma17194858